



Publication Year	2018
Acceptance in OA @INAF	2020-10-14T14:26:30Z
Title	SOLIS IV. Hydrocarbons in the OMC-2 FIR4 Region, a Probe of Energetic Particle Irradiation of the Region
Authors	Favre, C.; Ceccarelli, C.; López-Sepulcre, A.; FONTANI, FRANCESCO; Neri, R.; et al.
DOI	10.3847/1538-4357/aabfd4
Handle	http://hdl.handle.net/20.500.12386/27813
Journal	THE ASTROPHYSICAL JOURNAL
Number	859

SOLIS IV. HYDROCARBONS IN THE OMC–2 FIR 4 REGION, A PROBE OF ENERGETIC PARTICLE IRRADIATION OF THE REGION*

C. FAVRE,^{1,2} C. CECCARELLI,¹ A. LÓPEZ-SEPULCRE,^{1,3} F. FONTANI,² R. NERI,³ S. MANIGAND,^{1,4} M. KAMA,⁵ P. CASELLI,⁶ A. JABER AL-EDHARI,^{1,7} C. KAHANE,¹ F. ALVES,⁶ N. BALUCANI,⁸ E. BIANCHI,² E. CAUX,^{9,10} C. CODELLA,² F. DULIEU,¹¹ J. E. PINEDA,⁶ I. R. SIMS,¹² AND P. THEULÉ¹³

¹Univ. Grenoble Alpes, CNRS, IPAG, F-38000 Grenoble, France

²INAF-Osservatorio Astrofisico di Arcetri, Largo E. Fermi 5, I-50125, Florence, Italy

³Institut de Radioastronomie Millimétrique, 300 rue de la Piscine, 38406, Saint-Martin d'Hères, France

⁴Centre for Star and Planet Formation, Niels Bohr Institute & Natural History Museum of Denmark, University of Copenhagen, Øster Voldgade 5-7, 1350 Copenhagen K., Denmark

⁵Institute of Astronomy, University of Cambridge, Madingley Road, Cambridge CB3 0HA, UK

⁶Max-Planck-Institut für extraterrestrische Physik, Giessenbachstrasse 1, 85748 Garching, Germany

⁷University of AL-Muthanna, College of Science, Physics Department, AL-Muthanna, Iraq

⁸Dipartimento di Chimica, Biologia e Biotecnologie, Università di Perugia, Via Elce di Sotto 8, I-06123 Perugia, Italy

⁹Université de Toulouse, UPS-OMP, IRAP, Toulouse, France

¹⁰CNRS, IRAP, 9 Av. Colonel Roche, BP 44346, F-31028 Toulouse Cedex 4, France

¹¹LERMA, Université de Cergy-Pontoise, Observatoire de Paris, PSL Research University, CNRS, Sorbonne Université, UPMC Univ. Paris 06, École normale supérieure, France.

¹²Institut de Physique de Rennes, UMR CNRS 6251, Université de Rennes 1, 263 Avenue du Général Leclerc, F-35042 Rennes Cedex, France

¹³Aix-Marseille Université, PIIM UMR-CNRS 7345, 13397 Marseille, France

(Received July 1, 2016; Revised September 27, 2016; Accepted April 24, 2018)

Submitted to ApJ

ABSTRACT

We report new interferometric images of cyclopropenylidene, $c\text{-C}_3\text{H}_2$, towards the young protocluster OMC–2 FIR 4. The observations were performed at 82 and 85 GHz with the NOEMA as part of the project Seeds Of Life In Space (SOLIS). In addition, IRAM-30m data observations were used to investigate the physical structure of OMC–2 FIR 4. We find that the $c\text{-C}_3\text{H}_2$ gas emits from the same region where previous SOLIS observations showed bright HC_5N emission. From a non-LTE analysis of the IRAM-30m data, the $c\text{-C}_3\text{H}_2$ gas has an average temperature of ~ 40 K, a H_2 density of $\sim 3 \times 10^5 \text{ cm}^{-3}$, and a $c\text{-C}_3\text{H}_2$ abundance relative to H_2 of $(7 \pm 1) \times 10^{-12}$. In addition, the NOEMA observations provide no sign of significant $c\text{-C}_3\text{H}_2$ excitation temperature gradients across the region (about 3-4 beams), with T_{ex} in the range 8 ± 3 up to 16 ± 7 K. We thus infer that our observations are inconsistent with a physical interaction of the OMC–2 FIR 4 envelope with the outflow arising from OMC–2 FIR 3, as claimed by previous studies. The comparison of the measured $c\text{-C}_3\text{H}_2$ abundance with the predictions from an astrochemical PDR model indicates that OMC–2 FIR 4 is irradiated by a FUV field ~ 1000 times larger than the interstellar one, and by a flux of ionising particles ~ 4000 times larger than the canonical value of $1 \times 10^{-17} \text{ s}^{-1}$ from the Galaxy cosmic rays, which is consistent with our previous HC_5N observations. This provides an important and independent confirmation of other studies that one or more sources inside the OMC–2 FIR 4 region emit energetic (≥ 10 MeV) particles.

Corresponding author: C. Favre
cfavre@arcetri.astro.it

* Based on observations carried out under project number L15AA with the IRAM NOEMA Interferometer. IRAM is supported by INSU/CNRS (France), MPG (Germany) and IGN (Spain).

Keywords: ISM: abundances — ISM: clouds – ISM: molecules – Radio lines: ISM

1. INTRODUCTION

Earth is so far the only known place where life is present. Why life emerged and what conditions are essential for that are questions which challenge our knowledge and still represent a mystery. Very likely, life is the result of a very long and complex process that started as early as the formation of the Solar System (hereafter, SS). Sparse traces of the process have been left in the SS small bodies (e.g. Caselli & Ceccarelli 2012), so that to reconstruct it we need (also) to look at places that are forming Solar-type planetary systems today. However, finding such systems depends on the partial knowledge that we have of the history of the SS formation. In practice, therefore, reconstructing the SS past history has to be an “iterative” process.

Among the information provided by the mentioned SS left traces, two are particularly relevant for the work presented in this article. First, the Sun was most likely born in a crowded star cluster in the vicinity of high-mass stars, and not in an isolated cloud (e.g. Adams 2010). Second, it underwent a period of intense irradiation from energetic (≥ 10 MeV) particles, even though the cause is not clear yet (e.g. Gounelle et al. 2013).

When taking these two facts into account, the source OMC-2 FIR 4, north of the famous Orion KL region, is so far the best and closest analogue of the SS progenitor in our hands. Indeed available observations show that OMC-2 FIR 4 is a cluster of several young protostars (Shimajiri et al. 2011, 2015; López-Sepulcre et al. 2013b) and that it is permeated by a flux of energetic particles, cosmic-ray (CR) like, which ionise the molecular gas at a rate more than 4000 times the “canonical” value of $1 \times 10^{-17} \text{ s}^{-1}$ in the Galaxy (Ceccarelli et al. 2014; Fontani et al. 2017). Given the vicinity of the Trapezium OB star cluster, the region is also subject to a strong irradiation from FUV photons, about 1000 times larger than the interstellar field (López-Sepulcre et al. 2013a).

For these reasons, OMC-2 FIR 4 is one of the targets of the project Seeds Of Life In Space (SOLIS; Ceccarelli et al. 2017) whose goal is to understand how molecular complexity grows in Solar-type star forming systems. Within this project, we carried out observations with the IRAM NORthern Extended Millimeter Array (NOEMA) interferometer at various frequencies. A first study on the cyanopolyynes (HC_3N and HC_5N) showed that carbon chains growth is favoured in OMC-2 FIR 4, likely thanks to the presence of the large CR-like ionising particles flux (Fontani et al. 2017).

In this work, we present new SOLIS observations of the small hydrocarbon $c\text{-C}_3\text{H}_2$. The NOEMA SOLIS data are complemented with broad band IRAM-30m ob-

servations at 1, 2, and 3 mm. The article is organised as follows. Section 2 describes these new observations. We detected and imaged several lines as described in Section 3. With this large and diversified dataset, we could carry out a sophisticated analysis of the excitation conditions (Section 4) and the chemical structure (Section 5) of the region. In Section 6, we discuss the information provided by the new observations and the implications on the processes occurring in the OMC-2 FIR 4 region.

2. OBSERVATIONS AND DATA REDUCTION

We obtained observations of three $c\text{-C}_3\text{H}_2$ lines with the IRAM interferometer NOEMA within the SOLIS project (Ceccarelli et al. 2017). They are here complemented with IRAM 30m observations of several $c\text{-C}_3\text{H}_2$ lines, detected in the spectral survey previously carried out towards OMC-2 FIR 4 in the 3, 2 and 1 mm bands (López-Sepulcre et al. 2015). We present the two sets of observations separately.

2.1. SOLIS NOEMA observations

Three $c\text{-C}_3\text{H}_2$ lines, one para ($2_{0,2}\text{-}1_{1,1}$) and two ortho ($3_{1,2}\text{-}3_{0,3}$ and $2_{1,2}\text{-}1_{0,1}$), were imaged towards OMC-2 FIR 4 with the IRAM NOEMA interferometer. The first two lines, both at ~ 82 GHz, were observed with 6 antennas on 2015 August 5, 11, 12, 13 and 19 in the D configuration (see also Fontani et al. 2017). The third line, at 85 GHz, was observed with 8 antennas on 2016 April 29 and 2016 October 26 in the C configuration. All three lines were observed with the WideX band correlator, which provides 1843 channels over 3.6 GHz bandwidth with a channel width of 1.95 MHz ($\sim 7.2 \text{ km s}^{-1}$ at 82 GHz). Table 1 reports the spectroscopic data and the main characteristics of the observations.

The phase-tracking center was $\alpha_{J2000} = 05^{\text{h}}35^{\text{m}}26^{\text{s}}.97$, $\delta_{J2000} = -05^{\circ}09'56''.8$ for all data sets, and the systemic velocity of OMC2-FIR4 was set to $V_{LSR} = 11.4 \text{ km s}^{-1}$. The primary beams are about $61''$ and $59''$ for data at 82 GHz and 85 GHz, respectively. The nearby quasars 3C454.3 and 0524+034 were respectively used as bandpass calibrator and gain calibrator for the observations at 82 GHz. Regarding the observations performed at 85 GHz, 0524+024 and 0539-057 were used as gain (phase and amplitude) calibrators while 3C454.3 was used as bandpass calibrator. The absolute flux calibration was performed through observations of the quasars LKHA101 (0.21 Jy) for 2015 August 5 and 19, MWC349 (1.03 Jy) for 2015 August 11, 12 and 13 and again MWC349 (1.05 Jy) for 2016 observations.

Table 1. Properties of the cyclopropenylidene ($c\text{-C}_3\text{H}_2$) lines observed with the NOEMA interferometer: spectroscopic line parameters (transition, frequency, upper level energy and Einstein coefficient) and major characteristics of the observations (synthesized beam and P.A.).

Trans.	Freq. (MHz)	E_{up} (K)	A (10^{-5} s^{-1})	beam ($''$)	P.A. ($^\circ$)
para $c\text{-C}_3\text{H}_2$					
$2_{0,2}\text{-}1_{1,1}$	82093.544	6.4	2.1	9.3×5.9	-206
ortho $c\text{-C}_3\text{H}_2$					
$3_{1,2}\text{-}3_{0,3}$	82966.197	16.0	1.1	9.3×5.9	-206
$2_{1,2}\text{-}1_{0,1}$	85338.896	6.4	2.6	4.7×2.2	14

We used the spectroscopic data parameters from [Bogey et al. \(1986\)](#), [Vrtilek et al. \(1987\)](#), [Lovas et al. \(1992\)](#) and [Spezzano et al. \(2012\)](#), that are available from the Cologne Database for Molecular Spectroscopy molecular line catalog (CDMS, [Müller et al. 2005](#)). The Einstein coefficients assume an ortho-to-para ratio of 3:1.

Continuum subtraction and data imaging were performed using the GILDAS software¹. The cleaning of the spectral lines was performed by using the Hogbom method ([Högbom 1974](#)). The resulting synthesized beam size of the molecular emission maps are $9.5'' \times 6.1''$ (P.A. = -206°) and $4.7'' \times 2.2''$ (P.A. = 14°) at 82 GHz and 85 GHz, respectively. The NOEMA emission maps shown in this paper are corrected for primary beam.

2.2. IRAM-30m observations

Additional observations of the $c\text{-C}_3\text{H}_2$ lines were obtained in the context of the unbiased spectral survey of OMC-2 FIR 4 obtained with the IRAM 30m telescope. The 3 mm (80.5-116.0 GHz), 2 mm (129.2-158.8 GHz) and 1 mm (202.5-266.0 GHz) bands were observed between 31 Aug. 2011 and 7 Feb. 2014. The Eight Mixer Receiver (EMIR) connected to the 195 kHz resolution about 0.7 km s^{-1} at 83 GHz) Fourier Transform Spectrometer (FTS) units were used. The main beam sizes are about $9\text{-}12''$, $16''$ and $30''$ at 1, 2 and 3 mm, respectively. The observations were carried out in wobbler switch mode, with a throw of $180''$. Pointing and focus were performed regularly. The coordinates of the IRAM-30m observations are $\alpha_{J2000} = 05^{\text{h}}35^{\text{m}}26^{\text{s}}.97$ and $\delta_{J2000} = -05^\circ 09' 54''.5$. For further details, see [López-Sepulcre et al. \(2015\)](#).

We used the package CLASS90 of the GILDAS software collection to reduce the data. The uncertainties of

calibration are estimated to be lower than 10% at 3mm and 20% at 2 and 1mm. After subtraction of the continuum emission via first-order polynomial fitting, a final spectrum was obtained by stitching the spectra from each scan and frequency setting. The intensity was converted from antenna temperature (T_{ant}^*) to main beam temperature (T_{mb}) using the beam efficiencies provided at the IRAM web site for the epoch of the observations.

3. RESULTS

3.1. $c\text{-C}_3\text{H}_2$ emission maps

The NOEMA emission maps of the three $c\text{-C}_3\text{H}_2$ lines integrated over the line profile are shown in Figure 1 (panels a to c). The figure also displays the continuum emission (panel d), previously reported by [Fontani et al. \(2017\)](#), for reference.

$c\text{-C}_3\text{H}_2$ line emission is detected around FIR4, while FIR 3 and FIR5 do not show any emission above the 3σ level. The emission at 82 GHz towards FIR4 is rather extended with a hint that it could be associated with two compact sources north-west and south-east of FIR4, respectively. The map at 85 GHz, obtained with a higher spatial resolution, reveals emission in the same region as the one seen with the 82 GHz lines. Again, the emission is slightly clumpy (with 1σ difference between clumps). A forthcoming study, using higher spatial resolution continuum observations will address the level of core fragmentation in detail ([Neri et al. in preparation](#)).

Interestingly enough, the extended $c\text{-C}_3\text{H}_2$ 82 GHz emission is roughly co-spatial with that of HC_5N , (which was observed within the same frequency setting [Fontani et al. 2017](#)), rather than that of HC_3N as shown in Figure 2.

3.2. $c\text{-C}_3\text{H}_2$ single-dish emission

The 30m observations detected 24 $c\text{-C}_3\text{H}_2$ lines, 14 from the ortho form and 10 from para. Spectra of the $c\text{-C}_3\text{H}_2$ transitions observed with the IRAM 30-m telescope towards OMC-2 FIR 4 are displayed in Figures 8, 9 and 10 in Appendix A. Their properties are reported in Table 2. The lines are peaked around the ambient cloud velocity ($\sim 11 \text{ km s}^{-1}$) and are narrow (FWHM $\sim 1.0\text{-}1.6 \text{ km/s}$), indicating that they are emitted by the dense envelope surrounding FIR4 (see Sec. 4).

3.3. Missing flux

To estimate the fraction of the total flux that is filtered out in our interferometric data, we compared the NOEMA to the IRAM 30m lines. More specifically, the NOEMA spectra were convolved with a Gaussian beam similar to that of the 30m beam (i.e. $\sim 30''$ at 82-83 GHz). The convolution was performed at the central

¹ <http://www.iram.fr/IRAMFR/GILDAS/>

Table 2. c-C₃H₂ lines detected with the IRAM 30m telescope.

Freq. (GHz)	E_{up} (K)	A (10^{-5} s^{-1})	Intensity ^a K km/s	FWHM ^c km/s
80.7232	28.8	1.5	0.058 ± 0.006	1.6
82.0936^b	6.4	2.1	0.310 ± 0.030	1.6
82.9662^b	16.0	1.1	0.290 ± 0.030	1.5
84.7277	16.1	1.2	0.100 ± 0.010	1.5
85.3389^b	6.4	2.6	1.200 ± 0.120	1.4
85.6564	29.1	1.7	0.120 ± 0.010	1.4
150.4365	9.7	5.9	0.240 ± 0.050	1.2
150.8207	19.3	18.0	0.590 ± 0.120	1.2
150.8519	19.3	18.0	1.700 ± 0.340	1.2
151.0392	54.7	6.9	0.043 ± 0.009	1.1
151.3439	35.4	4.4	0.110 ± 0.020	1.1
151.3611	35.4	4.4	0.042 ± 0.008	1.1
155.5183	16.1	12.3	0.400 ± 0.080	1.1
204.7889	28.8	13.7	0.130 ± 0.030	1.1
216.2788	19.5	28.1	0.740 ± 0.150	1.0
217.8221	38.6	59.3	1.360 ± 0.270	1.2
217.9400	35.4	44.3	0.700 ± 0.140	1.1
218.1604	35.4	44.4	0.270 ± 0.050	1.1
227.1691	29.1	34.2	0.630 ± 0.120	1.0
244.2221	18.2	6.5	0.230 ± 0.050	1.2
249.0544	41.0	45.7	0.280 ± 0.060	1.1
251.3143	50.7	93.5	0.870 ± 0.170	1.2
254.9876	41.1	51.7	0.120 ± 0.020	1.0
260.4797	44.7	17.7	0.080 ± 0.020	1.1

We used the spectroscopic data parameters from [Bogey et al. \(1986\)](#), [Vrtilek et al. \(1987\)](#), [Lovas et al. \(1992\)](#) and [Spezzano et al. \(2012\)](#), that are available from the Cologne Database for Molecular Spectroscopy molecular line catalog (CDMS, [Müller et al. 2005](#)). The Einstein coefficients assume an ortho-to-para ratio of 3:1.

NOTES: ^aThe error in the intensity is the quadratic sum of the statistical and calibration errors. ^bThe emission from this line was imaged by NOEMA. ^cThe FWHM result from gaussian fit.

position of the IRAM 30m observations (see Sec. 2). Finally, the IRAM-30m spectra were smoothed to the same spectral resolution ($\sim 7.2 \text{ km s}^{-1}$) as that of the NOEMA WideX spectra. The comparison of the integrated line fluxes shows that 57% of the c-C₃H₂ 2_{0,2}-1_{1,1} emission, 60% of that of 3_{1,2}-3_{0,3} and 80% of that of 2_{1,2}-1_{0,1} lines is resolved out. Therefore, the c-C₃H₂ emission detected

by NOEMA very likely probes the densest part of the envelope surrounding FIR4 and not the ambient cloud.

4. TEMPERATURE AND C-C₃H₂ COLUMN DENSITY

4.1. Average properties of the FIR4 envelope

We first derive the average properties of the FIR4 envelope using the IRAM 30m data. To this end, we first carried out a simple LTE analysis, and then a non-LTE one.

4.1.1. LTE analysis

The rotational diagram, obtained assuming an ortho-to-para ratio equal to 3 and a beam filling factor equal to 1, is shown in Fig. 3. No systematic difference is seen between ortho and para lines, which implies that our assumption on the ortho-to-para ratio is basically correct.

The derived rotational temperature is $(12.6 \pm 0.5) \text{ K}$ and the c-C₃H₂ column density is $(7 \pm 1) \times 10^{12} \text{ cm}^{-2}$. Assuming that the emission arises from a 20'' region (see below), would not change much these results: it would give $(10.7 \pm 0.5) \text{ K}$ and $(1.5 \pm 0.2) \times 10^{13} \text{ cm}^{-2}$, respectively, and a slightly worse (but not significantly better) χ^2_{red} (0.08 instead of 0.05).

4.1.2. non-LTE analysis

Given the large number of c-C₃H₂ lines, we carried out a non-LTE analysis assuming the Large Velocity Gradient (LVG) approximation. To this end, we used the LVG code described in [Ceccarelli et al. \(2002\)](#) and used the collisional coefficients with He, after scaling for the different mass of H₂, computed by [Chandra & Kegel \(2000\)](#) and retrieved from the BASECOL database². We assumed a c-C₃H₂ ortho-to-para ratio equal to 3, as suggested by the LTE analysis.

We ran a large grid of models with H₂ density between 3×10^4 and $5 \times 10^6 \text{ cm}^{-3}$, temperature between 10 and 50 K and c-C₃H₂ column density between 3×10^{12} and $2 \times 10^{13} \text{ cm}^{-2}$. We adopted a FWHM of 1.3 km s^{-1} and let the filling factor be a free parameter. We then compared the LVG predictions with the observations and used the standard minimum reduced χ^2 criterium to constrain the four parameters: H₂ density, temperature, column density and size. In practice, for each column density we found the minimum χ^2 in the density-temperature-size parameter space. The solution then is the one with the c-C₃H₂ column density giving the smallest χ^2 .

² <http://basecol.obspm.fr>: [Dubernet et al. \(2013\)](#).

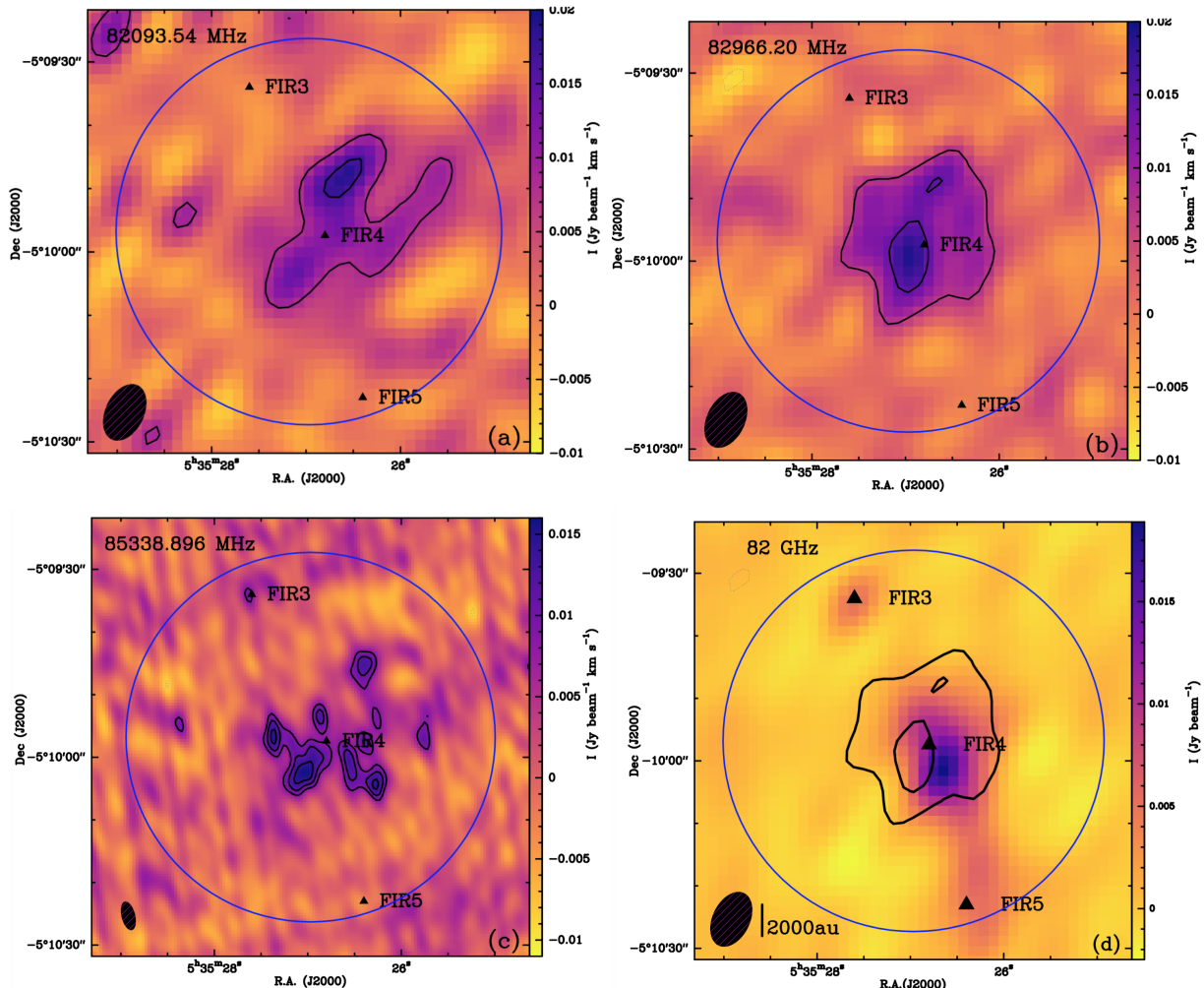


Figure 1. *Panel a:* $c\text{-C}_3\text{H}_2$ ($2_{0,2}\text{-}1_{1,1}$) integrated intensity emission map (between 0 and 22 km s^{-1}). The contour levels are at 3σ and 6σ (where $1\sigma=2.76\times 10^{-3}$ $\text{Jy beam}^{-1} \text{km s}^{-1}$). *Panel b:* $c\text{-C}_3\text{H}_2$ ($3_{1,2}\text{-}3_{0,3}$) integrated intensity emission map (between 0 and 22 km s^{-1}). The contour levels are at 3σ and 6σ (where $1\sigma=2.4\times 10^{-3}$ $\text{Jy beam}^{-1} \text{km s}^{-1}$). *Panel c:* $c\text{-C}_3\text{H}_2$ ($2_{1,2}\text{-}1_{0,1}$) integrated intensity emission map (between 0 and 22 km s^{-1}). The contour levels are at 3σ , 4σ and 5σ (where $1\sigma=2.8\times 10^{-3}$ $\text{Jy beam}^{-1} \text{km s}^{-1}$). *Panel d:* 82 GHz continuum emission (color) overlaid with the integrated intensity emission map of the $c\text{-C}_3\text{H}_2$ ($3_{1,2}\text{-}3_{0,3}$) at 82966 MHz (black contours). The contour levels for the continuum and $c\text{-C}_3\text{H}_2$ emission maps are the same as in Fontani et al. (2017) and in Panel b. Finally, in Panels a, b, c and d, the black triangles indicate the positions of the FIR3, FIR4 and FIR5 regions (see Chini et al. 1997); and the blue circle shows the NOEMA field of view.

The best fit is obtained for an extended source (i.e. $\geq 30''$), $c\text{-C}_3\text{H}_2$ column density equal to $(7\pm 1)\times 10^{12}$ cm^{-2} (in excellent agreement with the LTE estimate), temperature equal to 40 K and density equal to 3×10^5 cm^{-3} . At 2σ level, the solution becomes degenerate in the density-temperature parameter space. A family of solutions are possible, with the two extremes at 15 K and 5×10^6 cm^{-3} on one side, and 50 K and 2×10^5 cm^{-3} on the other side. Please note that, indeed, the coldest and densest solution provides a temperature close to the rotational temperature (13 K). This means that the apparent LTE distribution of the transition levels derived by the IRAM 30m line intensities is also obtained with

non-LTE conditions and the densities and temperatures mentioned above, included the best fit solution. Finally, in all cases, the lines are optically thin. In the following, we will use the best fit solution and we will associate the errors as follows: (40 ± 10) K and $(3\pm 1)\times 10^5$ cm^{-3} .

Assuming a H_2 column density measured from the continuum by Fontani et al. (2017), $\sim 10^{24}$ cm^{-2} , we obtain an average $c\text{-C}_3\text{H}_2$ abundance of $(7\pm 1)\times 10^{-12}$, assuming that $c\text{-C}_3\text{H}_2$ is present across the entire OMC-2 FIR4 region (Section 5).

4.2. The structure of the FIR4 envelope

The maps obtained with the NOEMA interferometer allow us to estimate the gas temperature and the $c\text{-C}_3\text{H}_2$

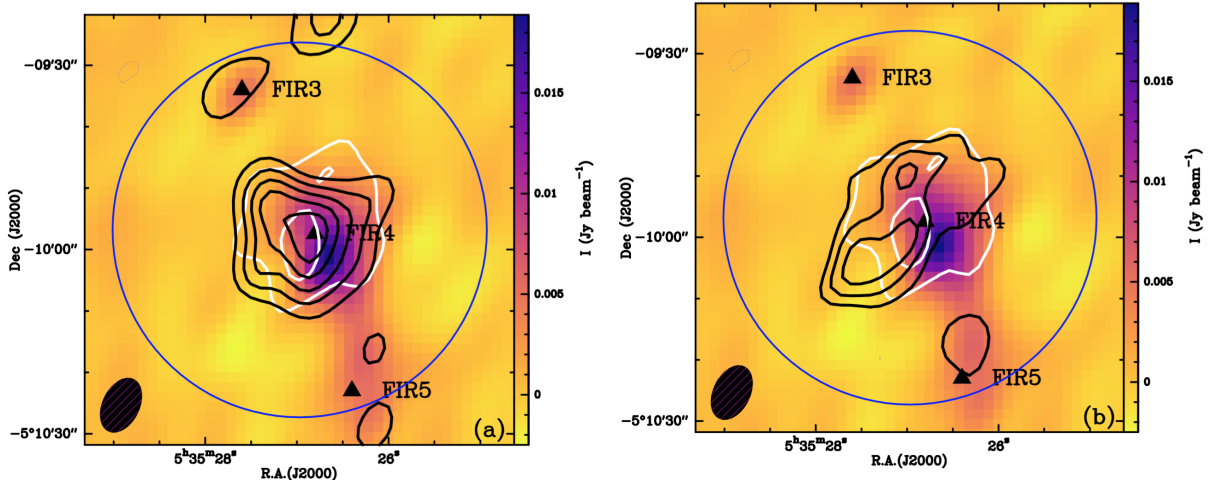


Figure 2. *Panel a:* 82 GHz continuum emission (color) overlaid with the integrated intensity emission map of the $c\text{-C}_3\text{H}_2$ ($3_{1,2}\text{-}3_{0,3}$) at 82.97 GHz (white contours) and that of the HC_3N (9–8) at 81.88 GHz (black contours; from Fontani et al. 2017). *Panel b* 82 GHz continuum emission (color) overlaid with the integrated intensity emission map of the $c\text{-C}_3\text{H}_2$ ($3_{1,2}\text{-}3_{0,3}$) at 82.97 GHz (white contours) and that of the HC_5N (31–30) at 82.54 GHz (black contours; from Fontani et al. 2017). Finally, in *Panels a and b*, the contour levels for the continuum, HC_3N and HC_5N maps are the same as in Fontani et al. (2017). Contour levels for the $c\text{-C}_3\text{H}_2$ emission map are given in Figure 1. The blue circle shows the NOEMA field of view.

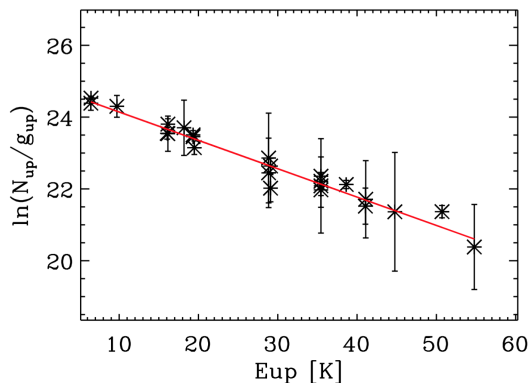


Figure 3. Rotational diagram derived from the $c\text{-C}_3\text{H}_2$ lines detected with the IRAM 30m telescope (Table 2). The ortho-to-para ratio is taken equal to 3. The error bars correspond to the 1σ Gaussian fit uncertainties.

abundance across the region probed by the NOEMA observations.

To measure the excitation temperature, we use the two $c\text{-C}_3\text{H}_2$ lines at 82 GHz, which have the same spatial resolution and, most importantly, the same amount of filtered out extended emission³. To this end, we assumed that (1) the $c\text{-C}_3\text{H}_2$ ortho-to-para ratio is equal to 3, (2) the lines are optically thin, and (3) the levels are LTE populated. With this assumptions, we derived the excitation temperature map shown in Figure

³ Please note that the 85 GHz line has a filtering twice larger than that of the lines at 82 GHz (Sec. 3.3).

4, along with the associated uncertainty. The excitation temperature is comprised between 8 ± 3 and 16 ± 7 K (i.e. minimum and maximum values, see Fig. 4). When considering the uncertainty on the values, there are no signs of excitation temperature gradients across the region we are probing (about 3-4 beams). On the contrary, the excitation temperature seems to be rather constant and not much different from that probed by the 30m data analysis (~ 12 K) (see previous section).

5. CHEMICAL MODELING

In the previous Section, we showed that the gas emitting the $c\text{-C}_3\text{H}_2$ lines has a temperature of ~ 40 K and H_2 density $\sim 3 \times 10^5 \text{ cm}^{-3}$. The $c\text{-C}_3\text{H}_2$ column density is $\sim 7 \times 10^{12} \text{ cm}^{-2}$. In this section, we use a Photo-Dissociation Region (PDR) model to understand the structure of the gas probed by the $c\text{-C}_3\text{H}_2$ lines, notably where they come from, and what constraints they provide.

To this end, we used the Meudon PDR code⁴ (version 1.5.2, see Le Petit et al. 2006; Bron et al. 2016). The code computes the steady-state thermal and chemical structure of a cloud irradiated by a FUV radiation field G_o and permeated by CR that ionise the gas at a rate ζ_{CR} . Relevant to the chemistry, the code computes the gas-phase abundances of the most abundant species, including $c\text{-C}_3\text{H}_2$. In our simulations, we adopted the density derived by the $c\text{-C}_3\text{H}_2$ non-LTE

⁴ The code is publicly available at <http://pdr.obspm.fr>.

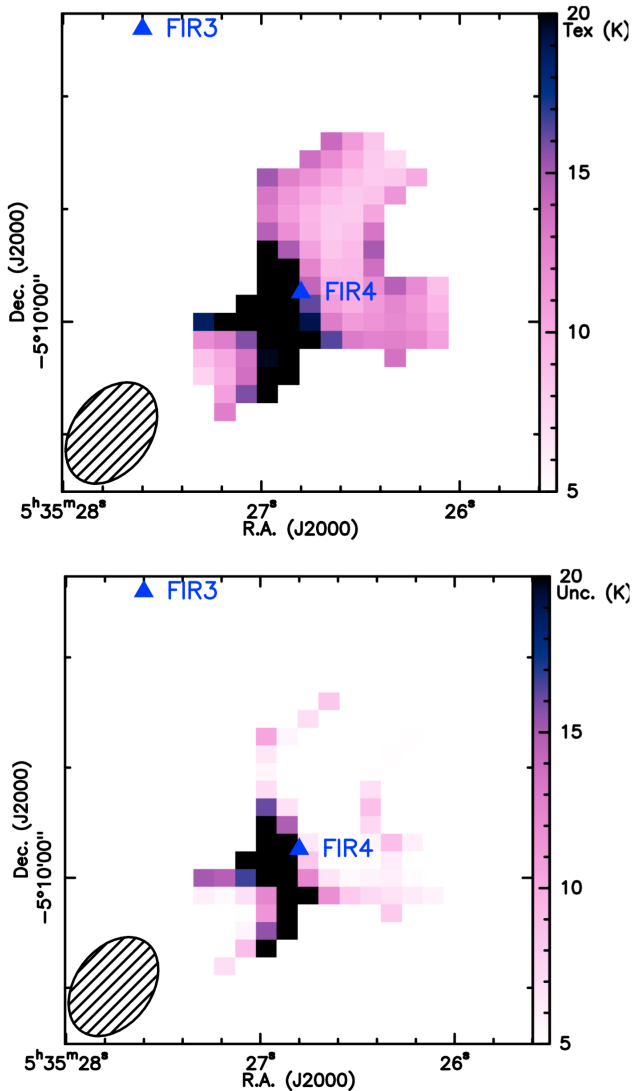


Figure 4. $c\text{-C}_3\text{H}_2$ excitation temperature map towards OMC2-FIR4 (top panel) along with the uncertainty map (bottom panel).

analysis ($n_H = 6 \times 10^5 \text{ cm}^{-3}$) and the elemental abundances listed in Table 3. Note that we limited the PDR simulations to a H-nuclei column density N_H of $\sim 4 \times 10^{22} \text{ cm}^{-2}$ (corresponding to $A_v=20$ mag; see Figs. 5 and 6). However, to compare the final predicted $c\text{-C}_3\text{H}_2$ column density, N_{Tot} , with the observed one ($7 \times 10^{12} \text{ cm}^{-2}$), we have to consider the whole cloud, which has a total H-nuclei column density N_H^{FIR4} of $2 \times 10^{24} \text{ cm}^{-2}$ (Fontani et al. 2017). Therefore, we multiplied the $c\text{-C}_3\text{H}_2$ abundance predicted by the model in the cloud interior $X_{interior}$ (computed by the code

Element	Abundance	Element	Abundance
O	3.2×10^{-4}	C	1.3×10^{-4}
N	7.5×10^{-5}	S	1.9×10^{-5}
Si	8.2×10^{-7}	Fe	1.5×10^{-8}

Table 3. Assumed elementary abundances, with respect to H nuclei, in the PDR modeling.

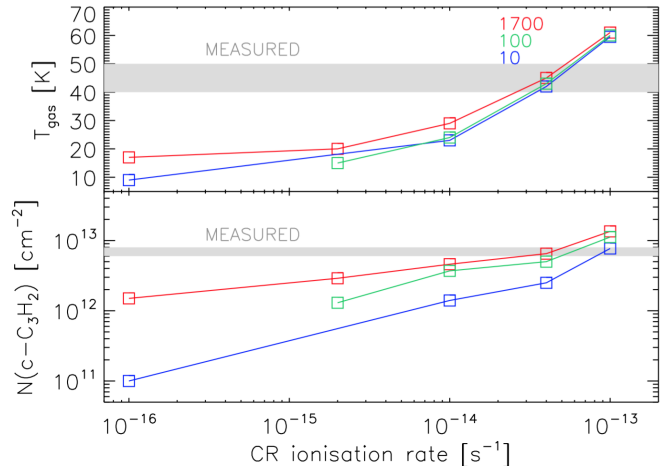


Figure 5. Results of the PDR modeling: predicted $c\text{-C}_3\text{H}_2$ column density (lower panel) and gas temperature (upper panel) as a function of the CR ionisation rate ζ_{CR} , for a FUV field G_0 equal to 1700 (red), 100 (green) and 10 (blue), respectively. Symbols show the actual runs.

at $N_H = 3 \times 10^{22} \text{ cm}^{-2}$)⁵ by N_H^{FIR4} , and added it to the $c\text{-C}_3\text{H}_2$ column density in the PDR region N_{PDR} (computed by the code for $N_H \leq 1 \times 10^{22} \text{ cm}^{-2}$), as follows:

$$N_{Tot} = X_{interior} \times N_H^{FIR4} + 2 \times N_{PDR} \quad (1)$$

To initialize our grid of models, we used as input parameter a temperature of 50 K, and assume an edge-on region that is irradiated from one side only. Then, we run several models with values of G_0 (G_0 is the FUV radiation field in Habing units⁶) ranging from 1 to 1700, and ζ_{CR} from $1 \times 10^{-16} \text{ s}^{-1}$ to $4 \times 10^{-14} \text{ s}^{-1}$. These extreme values are quoted in the literature for the OMC-2 region (see Introduction and Discussion). Note that, even though we did not run a full grid of models,

⁵ Please note that we used the $c\text{-C}_3\text{H}_2$ abundance at $N_H = 3 \times 10^{22} \text{ cm}^{-2}$ to avoid the region where opacities and, consequently, temperatures decrease because of the artificial boundary of the cloud.

⁶ $G_0 = 1$ corresponds to a FUV energy density of $5.3 \times 10^{-14} \text{ erg cm}^{-3}$. The interstellar standard radiation field is $G_0 = 1.7$.

Model	ζ_{CR} (10^{-16} s^{-1})	G_0	N_{PDR} (10^{12} cm^{-2})	$X_{interior}$	N_{Tot} (10^{12} cm^{-2})	T_{gas} (K)
1	1	1	0.01	9.8×10^{-16}	0.02	9
2	1	10	0.05	1.5×10^{-15}	0.1	9
3	1	1700	0.75	2.5×10^{-14}	1.5	17
4	20	100	0.11	5.3×10^{-13}	1.3	14
5	20	1700	0.77	7.1×10^{-13}	2.9	20
6	100	10	0.12	5.7×10^{-13}	1.4	23
7	100	100	0.18	1.6×10^{-12}	3.7	25
8	100	1700	0.79	1.5×10^{-12}	4.6	29
9	400	1	0.06	7.4×10^{-13}	1.6	41
10	400	10	0.19	1.1×10^{-12}	2.5	42
11	400	100	0.26	2.2×10^{-12}	5.0	43
12	400	1700	0.86	2.4×10^{-12}	6.5	45

Table 4. List of the ζ_{CR} and G_0 values adopted for the different PDR models and the results of the simulations: the $c\text{-C}_3\text{H}_2$ column density in the PDR region, N_{PDR} ; the $c\text{-C}_3\text{H}_2$ abundance (with respect to H nuclei) in the interior (see text), $X_{interior}$; the total $c\text{-C}_3\text{H}_2$ column density, N_{Tot} , which takes into account the whole cloud (see text); the gas temperature (in the interior).

we fine-tuned the parameter ranges close to the best fit solution.

The run models and the associated results are listed in Table 4 and shown in Figure 5. Both the predicted $c\text{-C}_3\text{H}_2$ column density and gas temperature are strong functions of ζ_{CR} : the larger ζ_{CR} the larger the column density and the temperature. On the contrary, the value of G_0 has a small influence on the predicted values, in particular for the temperature.

The comparison of the PDR modeling results (Table 4 and Figure 5) with the measured $c\text{-C}_3\text{H}_2$ column density and gas temperature very clearly indicates that the gas is permeated by a large flux of CR and is irradiated by an intense FUV field. Specifically, model 12 ($\zeta_{CR} = 4 \times 10^{-14} \text{ s}^{-1}$ and $G_0 = 1700$) reproduces fairly well the measured $c\text{-C}_3\text{H}_2$ column density ($\sim 7 \times 10^{12} \text{ cm}^{-2}$) and gas temperature ($\sim 40 \text{ K}$).

Figure 6 shows the gas temperature, the $c\text{-C}_3\text{H}_2$ abundance and column density as a function of $N(\text{H}+2\times\text{H}_2)$ for the model 12, which best reproduces the observations, and model 2, for comparison.

In general, the $c\text{-C}_3\text{H}_2$ abundance has a first peak in the PDR region, in a tiny layer at $N(\text{H}+2\times\text{H}_2) \leq \times 10^{21} \text{ cm}^{-2}$. This first peak depends on the FUV radiation field and increases with increasing G_0 . In the interior of the cloud, at $N(\text{H}+2\times\text{H}_2) \geq \times 10^{22} \text{ cm}^{-2}$, namely in the region that contributes most to the total $c\text{-C}_3\text{H}_2$ column density, the $c\text{-C}_3\text{H}_2$ abundance is governed by the CR ionisation rate and increases with ζ_{CR} . As expected, the gas temperature at the PDR border is governed by the

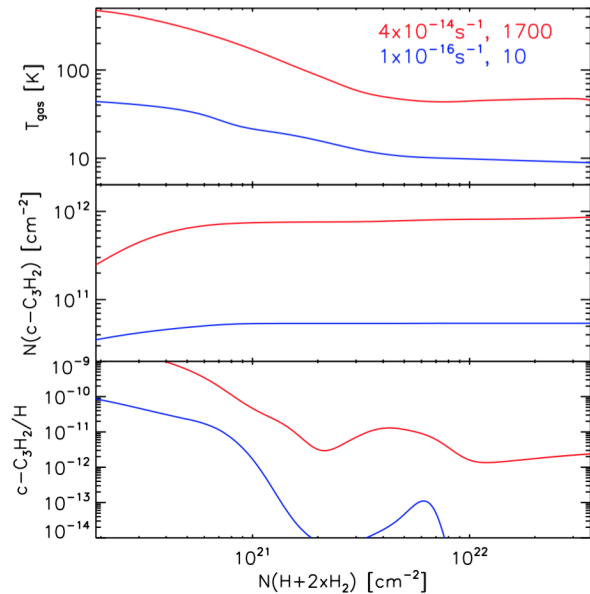


Figure 6. Thermal and chemical structure of two models: predicted gas temperature (upper panel), $c\text{-C}_3\text{H}_2$ column density in the PDR (middle panel) and abundance (bottom panel) as a function of the H nuclei column density. Two models are reported: model 12 ($\zeta_{CR} = 4 \times 10^{-14} \text{ s}^{-1}$ and $G_0 = 1700$; red), and model 2 ($\zeta_{CR} = 1 \times 10^{-16} \text{ s}^{-1}$ and $G_0 = 10$; blue).

FUV field, whereas it is governed by CR ionisation rate in the interior.

6. DISCUSSION

6.1. OMC-2 FIR 4: a highly irradiated region

In the previous section, we showed that in order to reproduce the temperature of the gas probed by the $c\text{-C}_3\text{H}_2$ lines and its abundance the gas has to be irradiated by a strong flux of CR-like particles. Amazingly, the best agreement between observations and model predictions is given by a CR ionisation rate, $\zeta_{CR} = 4 \times 10^{-14} \text{ s}^{-1}$, that is the same as the one derived by the following observations: (1) the HCO^+ and N_2H^+ high J lines observed by Herschel HIFI CHESS project (Ceccarelli et al. 2014), and (2) the HC_3N and HC_5N lines observed by NOEMA SOLIS project (Fontani et al. 2017). In addition, the $c\text{-C}_3\text{H}_2$ emitting region roughly coincides with the largest ζ_{CR} region which is probed by the HC_5N emission area. We emphasise that, in addition to being different data sets and different species, the three estimates of ζ_{CR} have been obtained also with three different astrochemical codes: ASTROCHEM⁷, Nahoon (Wakelam et al. 2012) and Meudon PDR (version 1.5.2, Le Petit et al. 2006; Bron et al. 2016) codes.

The emerging picture is shown in the cartoon of Figure 7. Previous Herschel HIFI CHESS observations showed that between OMC-2 and us there is a tenuous (100 cm^{-3}) cloud extending about 6 pc along the line of sight, and illuminated by a FUV field about 1000 times brighter than the interstellar standard radiation field (López-Sepulcre et al. 2013a). OMC-2 itself hosts three FIR sources (FIR 3, 4 and 5), which are likely very different in nature and evolutionary status, even though not much is known especially about FIR3 and FIR5, except that a large-scale ($\sim 30''$) outflow emanates from FIR3 (Takahashi et al. 2008; Shimajiri et al. 2008, 2015). FIR4 is actually a dense clump ($\sim 10^5 - 10^6 \text{ cm}^{-3}$; Crimier et al. 2009; Ceccarelli et al. 2014) with an embedded cluster of young sources, whose number is still unclear (Shimajiri et al. 2008; López-Sepulcre et al. 2013b; Kainulainen et al. 2017). What is clear now is that FIR4 is permeated by a flux of CR-like ionising particles about 1000 times larger than the CR flux of the Galaxy. The source(s) of these particles is(are) likely situated in the East part of FIR4 (Fontani et al. 2017), but still remains unidentified. Incidentally, it is important to note that the high CR ionization rate could result in a temperature gradient in the vicinity of the CR emitting source(s). Nonetheless, the $c\text{-C}_3\text{H}_2$ excitation temperature mainly covers the west region (see Figure 4), where the irradiation is likely lower, based on the $\text{HC}_5\text{N}/\text{HC}_3\text{N}$ abundance ratio by Fontani et al. (2017). The new IRAM 30m and SOLIS observations

presented in this work confirm this geometry and indicate that abundant hydrocarbons ($c\text{-C}_3\text{H}_2$) are present not only at the skin of the FIR4 clump but also in the interior, because of the strong CR-like irradiation.

6.2. No evidence of the FIR3 outflow impact on FIR4

It has been suggested that the chemical composition of OMC-2 FIR4 is affected by the interaction of the northeast-southwest outflow driven by the nearby source FIR3 (see Shimajiri et al. 2008, 2015), which is located at about $23''$ northeast from FIR4 (i.e. $\sim 9660 \text{ AU}$ at a distance of 420 pc, Menten et al. 2007; Hirota et al. 2007). Specifically, Shimajiri et al. (2008, 2015) have suggested that gas associated with OMC-2 FIR4 might be impacted by this NE-SW outflow. If this is the case, the gas associated with the envelope of the OMC-2 FIR4 region should show some physically induced effect. In this instance, the $c\text{-C}_3\text{H}_2$ molecular emission map would likely present a temperature gradient within the region. This is not the case in our observations (see Figure 4) which, contrary to Shimajiri et al. (2015), probe the envelope of OMC-2 FIR4 and not the ambient gas thanks to the interferometer spatial filtering. These findings lead one to ask whether the apparent spatial coincidence of the southern outflow lobe driven by FIR3 and the northern edge of FIR4 is simply a projection effect. More sensitive, higher angular resolution observations may help us confirm our current conclusion.

7. CONCLUSIONS

We have imaged, for the first time, the distribution of cyclopropenylidene, $c\text{-C}_3\text{H}_2$, towards OMC-2 FIR 4 with an angular resolution of $9.5'' \times 6.1''$ at 82 GHz and $4.7'' \times 2.2''$ at 85 GHz, using NOEMA. The observations were performed as part of the SOLIS program. In addition, we have performed a study of the physical properties of this source through the use of IRAM-30m observations.

Our main results and conclusions are the following:

1. From a non-LTE analysis of the IRAM-30m data, we find that $c\text{-C}_3\text{H}_2$ gas emits at the average temperature of about 40 K with a $\chi(c\text{-C}_3\text{H}_2)$ abundance of $(7 \pm 1) \times 10^{-12}$.
2. Our NOEMA observations show that there is no sign of excitation temperature gradients within the observed region (which corresponds to $\sim 3\text{-}4$ beams), with a $T_{ex}(c\text{-C}_3\text{H}_2)$ in the range $8 \pm 3 - 16 \pm 7 \text{ K}$. Our findings suggest that the OMC-2 FIR 4 envelope is not in direct physical interaction with the outflow originating from OMC-2 FIR 3.

⁷ <http://smaret.github.com/astrochem/>

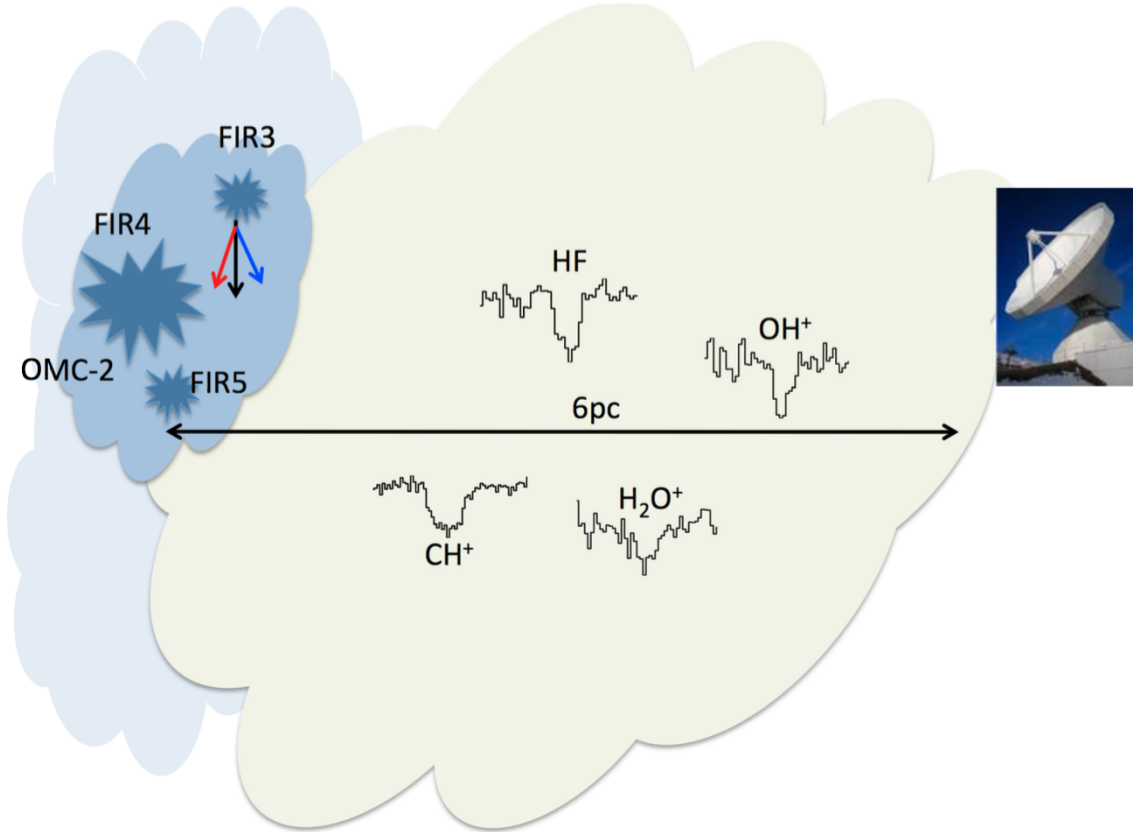


Figure 7. Cartoon of OMC-2. A tenuous cloud between OMC-2 and the Sun is probed by the absorption of HF, OH⁺, CH⁺ and H₂O⁺ observed by the Herschel HIFI instrument (López-Sepulcre et al. 2013a). The OMC-2 complex is associated with three FIR sources: FIR3, FIR4 and FIR5, respectively. An outflow is emitted by FIR3 which, based on the present observations, is unlikely impacting the FIR4 envelope.

3. In addition, the *c*-C₃H₂ gas probed by NOEMA arises from the same region as that of HC₅N which is a probe of high CR-particles ionization (Fontani et al. 2017).
4. Finally, a notable result, derived from chemical modelling with the Meudon PDR code is that OMC-2 FIR 4 appears to be a strongly irradiated region: FUV field dominates the outer shells (with a radiation field scaling factor G_0 of about 1700) while the interior of the envelope is governed by CR ionization (with a CR ionization rate $\zeta_{CR} = 4 \times 10^{-14} \text{ s}^{-1}$, namely more than a thousand times the canonical value).

These results are consistent with previous studies claiming that OMC-2 FIR 4 bathes in an intense radiation field of energetic particles ($\geq 10 \text{ MeV}$).

8. ACKNOWLEDGEMENTS

We warmly thank Franck Le Petit for his assistance in the use of the PDR code. CF acknowledge the financial support for this work provided by the French space agency CNES along with the support from the Italian Ministry of Education, Universities and Research, project SIR (RBSI14ZRHR). We acknowledge the funding from the European Research Council (ERC), projects PALs (contract 320620) and DOC (contract 741002). This work was supported by the French program Physique et Chimie du Milieu Interstellaire (PCMI) funded by the Conseil National de la Recherche Scientifique (CNRS) and Centre National d’Etudes Spatiales (CNES) and by the Italian Ministero dell’Istruzione, Università e Ricerca through the grant Progetti Premiali 2012 - iALMA (CUP C52I13000140001).

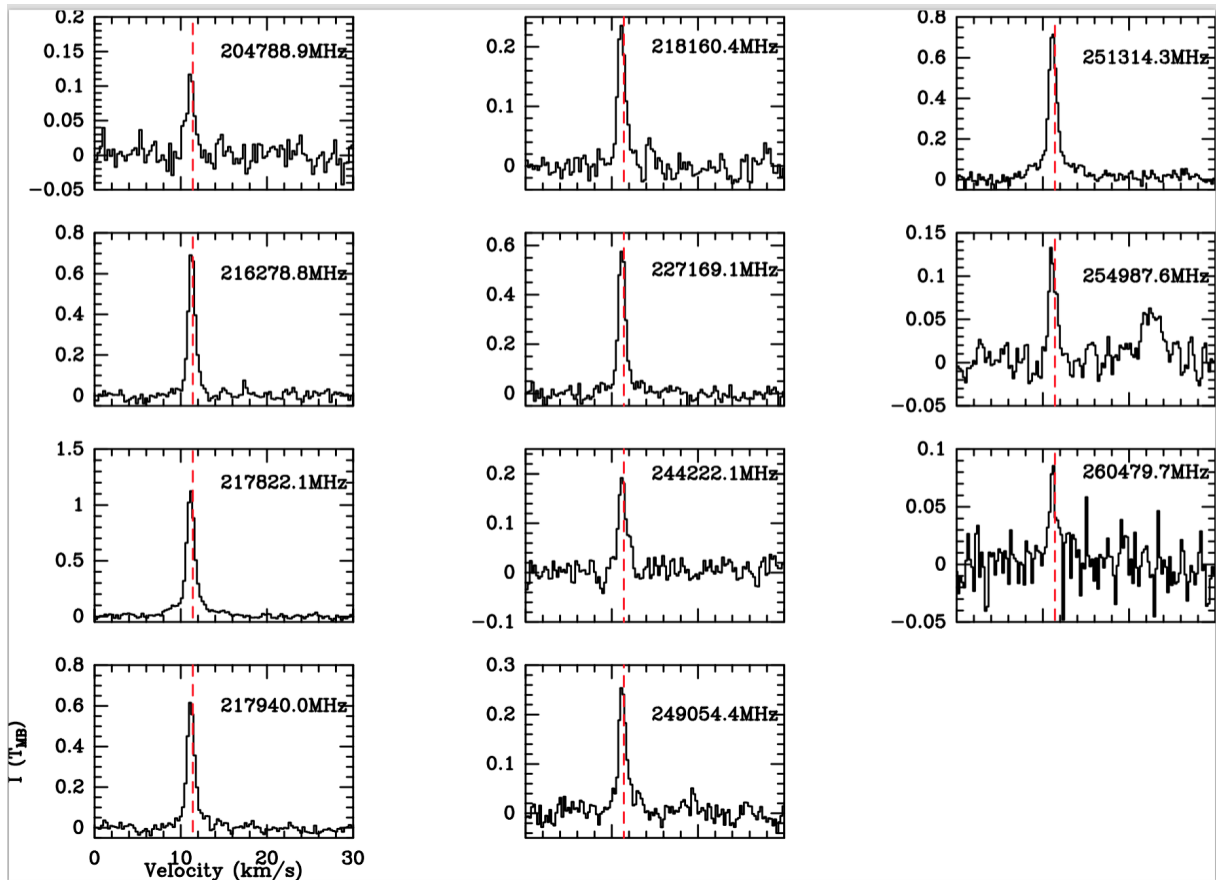


Figure 8. $c\text{-C}_3\text{H}_2$ spectra observed towards OMC-2 FIR 4 at 1 mm with the IRAM 30-m telescope. Dashed red lines indicate a $V_{LSR} = 11.4 \text{ km s}^{-1}$. The frequency the observed transition is indicated on each plot.

APPENDIX

A. $C\text{-C}_3\text{H}_2$ TOWARDS OMC-2 FIR 4 AS OBSERVED WITH IRAM-30M TELESCOPE

Figures 8 to 10 display the spectra of the $c\text{-C}_3\text{H}_2$ transitions observed with the IRAM 30-m telescope towards OMC-2 FIR 4 at 1, 2 and 3 mm, respectively.

REFERENCES

- Adams, F. C. 2010, *ARA&A*, 48, 47
- Bogey, M., Demuynck, C., & Destombes, J. L. 1986, *Chemical Physics Letters*, 125, 383
- Bron, E., Le Petit, F., & Le Bourlot, J. 2016, *A&A*, 588, A27
- Caselli, P., & Ceccarelli, C. 2012, *A&A Rv*, 20, 56
- Ceccarelli, C., Dominik, C., López-Sepulcre, A., et al. 2014, *ApJL*, 790, L1
- Ceccarelli, C., Baluteau, J.-P., Walmsley, M., et al. 2002, *A&A*, 383, 603
- Ceccarelli, C., Caselli, P., Fontani, F., et al. 2017, *ApJ*, 850, 176
- Chandra, S., & Kegel, W. H. 2000, *A&AS*, 142, 113
- Chini, R., Reipurth, B., Ward-Thompson, D., et al. 1997, *ApJL*, 474, L135
- Crimier, N., Ceccarelli, C., Lefloch, B., & Faure, A. 2009, *A&A*, 506, 1229
- Dubernet, M.-L., Alexander, M. H., Ba, Y. A., et al. 2013, *A&A*, 553, A50
- Fontani, F., Ceccarelli, C., Favre, C., et al. 2017, *A&A*, 605, A57
- Gounelle, M., Chaussidon, M., & Rollion-Bard, C. 2013, *ApJL*, 763, L33
- Hirota, T., Bushimata, T., Choi, Y. K., et al. 2007, *PASJ*, 59, 897
- Högbom, J. A. 1974, *A&AS*, 15, 417

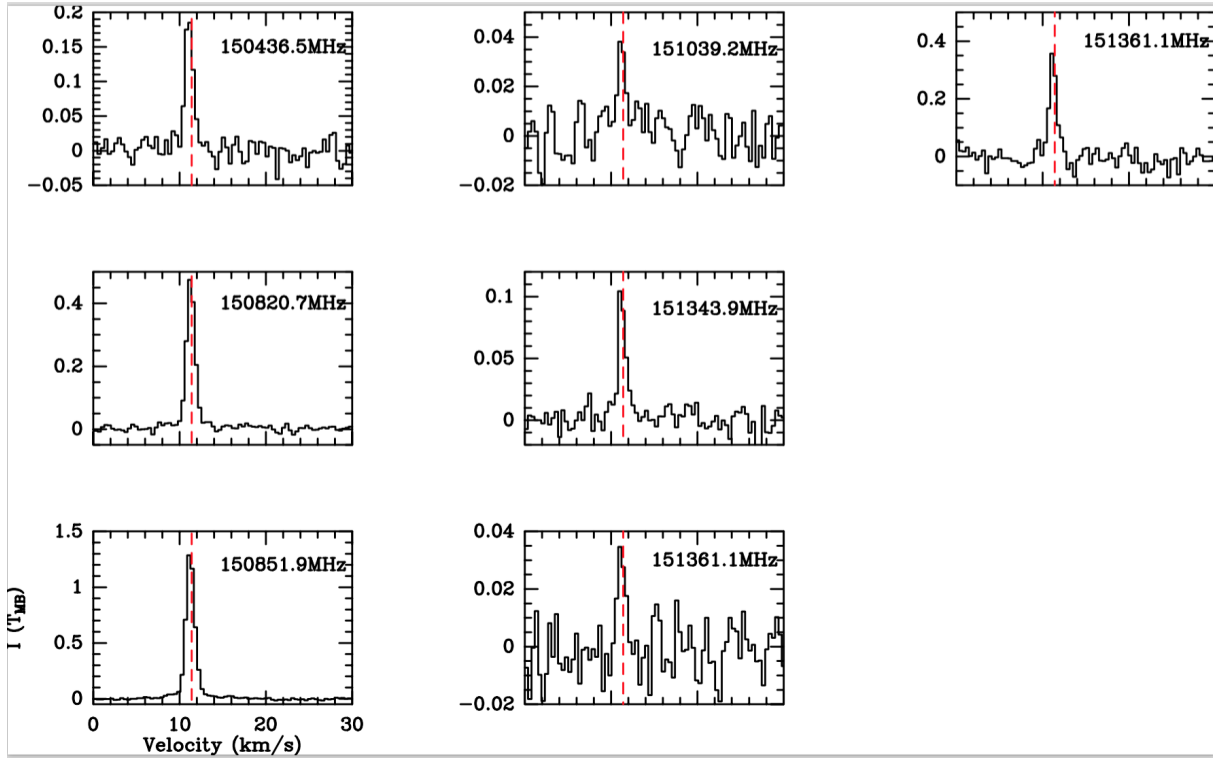


Figure 9. $c\text{-C}_3\text{H}_2$ spectra observed towards OMC-2 FIR 4 at 2 mm with the IRAM 30-m telescope. Dashed red lines indicate a $V_{LSR} = 11.4 \text{ km s}^{-1}$. The frequency the observed transition is indicated on each plot.

Kainulainen, J., Stutz, A. M., Stanke, T., et al. 2017, *A&A*, 600, A141

Le Petit, F., Nehmé, C., Le Bourlot, J., & Roueff, E. 2006, *ApJS*, 164, 506

López-Sepulcre, A., Kama, M., Ceccarelli, C., et al. 2013a, *A&A*, 549, A114

López-Sepulcre, A., Taquet, V., Sánchez-Monge, Á., et al. 2013b, *A&A*, 556, A62

López-Sepulcre, A., Jaber, A. A., Mendoza, E., et al. 2015, *MNRAS*, 449, 2438

Lovas, F. J., Suenram, R. D., Ogata, T., & Yamamoto, S. 1992, *ApJ*, 399, 325

Menten, K. M., Reid, M. J., Forbrich, J., & Brunthaler, A. 2007, *A&A*, 474, 515

Müller, H. S. P., Schlöder, F., Stutzki, J., & Winnewisser, G. 2005, *Journal of Molecular Structure*, 742, 215

Shimajiri, Y., Takahashi, S., Takakuwa, S., Saito, M., & Kawabe, R. 2008, *ApJ*, 683, 255

Shimajiri, Y., Kawabe, R., Takakuwa, S., et al. 2011, *PASJ*, 63, 105

Shimajiri, Y., Sakai, T., Kitamura, Y., et al. 2015, *ApJS*, 221, 31

Spezzano, S., Tamassia, F., Thorwirth, S., et al. 2012, *ApJS*, 200, 1

Takahashi, S., Saito, M., Ohashi, N., et al. 2008, *ApJ*, 688, 344

Vrtilek, J. M., Gottlieb, C. A., & Thaddeus, P. 1987, *ApJ*, 314, 716

Wakelam, V., Herbst, E., Loison, J.-C., et al. 2012, *ApJS*, 199, 21

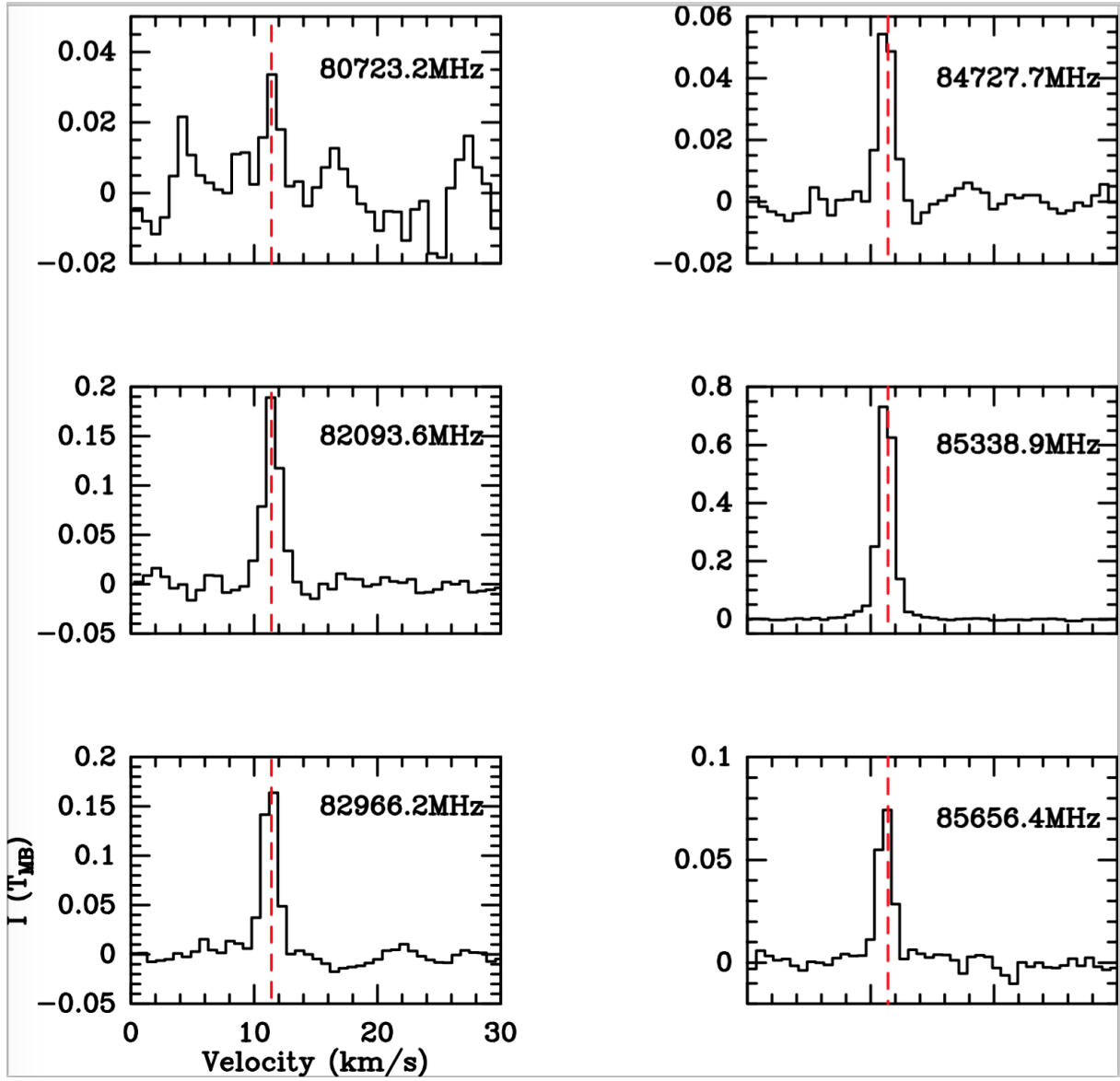


Figure 10. c - C_3H_2 spectra observed towards OMC-2 FIR 4 at 3 mm with the IRAM 30-m telescope. Dashed red lines indicate a $V_{LSR} = 11.4 km s^{-1}$. The frequency the observed transition is indicated on each plot.